Optimization of back contact grid size in Al_2O_3-rear-passivated ultra-thin CIGS PV cells by 2D simulations

J. Lontchi[1*], M. Zhukova[1], M. Kovacic[2], J. Krc[2], W.-C. Chen[3], M. Edoff[3], S. Bose[4], P. M. P. Salomé[4], J. Goffard[5], A. Cattoni[5], L. Gouillart[5], S. Collin[5], V. Gusak[6], D. Flandre[1]

[1]*Institute of Information and Communication Technologies, Electronics and Applied Mathematics, Université catholique de Louvain, 1348 Louvain-la-Neuve, Belgium*
[2]*University of Ljubljana, Faculty of Electrical Engineering, Trzaska 25, 1000 Ljubljana, Slovenia*
[3]*Uppsala University, dep. Eng. Sciences, Ångström lab, p.o. box 534, 751 21 Uppsala, Sweden*
[4]*International Iberian Nanotechnology Laboratory, 4715-330 Braga, Portugal*
[5]*Centre for Nanoscience and Nanotechnology, CNRS, University Paris-Sud/Paris-Saclay, 91120 Palaiseau, France*
[6]*Solibro Research AB, Vallvägen 5, 75651 Uppsala, Sweden*

**Corresponding author: jackson.lontchi@uclouvain.be*

Abstract

We present a simulation strategy using ATLAS-2D to optimize the back-contact hole grid (i.e. size and pitch of openings) of the Al_2O_3-rear-passivation layer in ultra-thin CIGS photovoltaic cells. We first discuss and compare our simulation model with a series of experimental reference (i.e. non passivated) and passivated UT-CIGS cells to decouple the crucial parameters of the passivation. The simulation results follow the experimental trends both for the current in the dark and for the PV parameters under illumination, highlighting the beneficial effects of the passivation on the cell performances. Furthermore, it stresses the influence of the passivation quality at the Al_2O_3/CIGS interface and of the contact resistance at the Mo/CIGS interface within the openings. Further simulations quantify significant improvements in short-circuit current and open-circuit voltage for different sizes of openings in the Al_2O_3 layer, relative to an excellent passivation quality (i.e. high density of negative charges in the passivation layer). However, a degradation of performances is predicted for a poor passivation (i.e. low density of such charges) or a high contact resistance, when compared to reference cells. Consequently, we point out an optimum in efficiency when varying the opening widths at fixed hole pitch and fixed contact resistance. At equivalent contact resistance, simulations predict that the sizes of the pitch and openings can be increased without optimal performance losses when maintaining a width to pitch ratio around 0.2. This simulation trend has been confirmed by a series of experiments, indicating that it is crucial to care about the dimensions of the opening grid and the contact resistance of passivated cells apart from different material properties. These simulation results provide significant insights for optimal cell design and characterizations of passivated UT-CIGS PV cells.

Keywords: *PV cells, ultra-thin CIGS, 2D modelling, opening/pitch, Al_2O_3 passivation, electrical characterization*

1. Introduction

Nowadays, ultra-thin Cu(In, Ga)Se_2 (UT-CIGS) technology is widely investigated for low-cost fabrication, low material usage and for flexible photovoltaic (PV) and Building integrated photovoltaic applications [1, 2]. However, lowering the thickness of the absorber layer below the standard micrometer scale reduces the light absorption and reveals degradation mechanisms that limit the PV performances of the cell [3, 4]. Therefore, engineering the ultra-thin cells, requires high-precision optimization methods to improve the performances to the level of the standard thicker cells.

Many researches have proposed different optimization approaches to increase the performances of UT-CIGS PV cells. The group at Uppsala university has reported on several experiments with grading of the CIGS absorber layer by different Ga/(In+Ga) ratios [5-8]. They reported the beneficial effect of the Ga-grading on a 0.5 µm thick CIGS cell with an improvement in absolute value of efficiency (*Eff*) around 2.5% due to an increase of the open-circuit voltage (*V*oc) and fill-factor (*FF*) values [5] with the possibility to engineer the bandgap by means of evaporation profile variations [6]. In collaboration with the Uppsala group, R. Kotipalli *et al.* in UCLouvain have reported a decrease of deep defects near the space charge region which was found to be beneficial for improving the *V*oc [9]. Several works reported the passivation of the Mo/CIGS interface by the introduction of a very thin oxide layer [10-17]. The main effect is the reduction of the rear recombination of photogenerated carriers that leads to an increase of the short-circuit current (*J*sc) and the *V*oc especially for ultra-thin cells [18, 19]. Another largely investigated approach is the intentional introduction of alkali elements to improve the transport properties and the resulted performance of thin CIGS PV cells [20, 21]. Moreover, to compensate the decrease of the absorption due to thickness reduction of the CIGS layer, researchers proposed the introduction of a rear optical reflector materials to reflect the non-absorbed incident light back into the CIGS to improve the *J*sc [22-26]. Other solutions to decrease the optical losses include improving front transparent contacts, usage of anti-reflection structures, introduction of textures and others [27]. Implementing different approaches to achieve high performances requires high-level engineering, a lot of time and expensive experiments. Therefore, simulations are helpful to reproduce, as accurately as possible, the experimental cell structures and measurement results by implementation of different parameters and different designs. Several papers have been already reported on simulations of thin and UT-CIGS PV cells with significant results on the effects of various properties on the cell performances [28-32]. B. Vermang *et al.* reported on Al_2O_3 rear-passivated thick CIGS cell with nano-sized local rear point contacts [11] that show a significant improvement in Voc compared to reference (i.e. non passivated) cells. However, the influence of the fixed charge density at the rear passivation layer along with the dimensions of the rear contact holes (i.e. size and pitch of opening grid) and the effect of the contact resistance have not yet been investigated in UT-CIGS PV cells.

We present in this paper a 2D model of reference and Al_2O_3-rear-passivated UT-CIGS cells built with ATLAS-2D simulation tool. We first discuss and compare the general trends of simulation results to the experimental cell results in the dark and their correlations with the PV parameters under illumination. We next discuss the concurrent influence of the passivation quality and of the contact resistance on the performance of the passivated cells for different opening sizes. The last section deals with the optimization of the opening width to pitch ratio in the passivated layer using the full 2D model simulation results, compared to experiments.

A final aim of the study is to show that a suitable 2D modelling can help to understand the performances of the Al_2O_3-rear-passivated UT-CIGS cells with regards to the size of the back-contact grid; furthermore, how it can provide useful predictions, trends and directions for their optimal design and accurate characterization, as well as to revisit contradictory results sometimes observed in experiments.

2. Study details:

2.1. Experiments details

The first experimental cells used in this work have been realized by different research groups within the European H2020 ARCIGS-M project. They consist of a series of reference and Al_2O_3-rear-passivated UT-CIGS cell with 500 nm CIGS thickness fabricated on soda lime glass (SLG) substrates at the International Iberian Nanotechnology Laboratory (INL).

Reference cells consist of SLG/(Mo, $MoSe_2$)/500 nm-CIGS/50 nm-CdS/100 nm-i:ZnO/300 nm-Al:ZnO with Ni/Al/Ni as front contact. For passivated cells, a 25 nm thin layer of Al_2O_3 has been deposited on top of Mo before the CIGS deposition. A grid of contact holes has been opened within the Al_2O_3 layer with a diameter (W = 200 nm) and an equidistant hole pitch (P = 2 µm). Details about fabrication process can be found at the reference [33].

Another series of reference and Al_2O_3-rear-passivated UT-CIGS cells with different hole pitches have been fabricated on SLG substrates at the Centre for Nanoscience and Nanotechnology (CNRS) with the collaboration of Solibro Research AB (Solibro). The structure of the reference cell is the same as in the previous series from INL (SLG/Mo/CIGS/CdS/i:ZnO/Al:ZnO/(Ni/Al/Ni)) while the Al_2O_3 layer in passivated cells has various contact hole patterns. The diameter of the openings has been kept constant (W = 300 nm) but the distance between the centres of two adjacent holes (pitch) has been varied from 1 µm to 4 µm. The aim was to investigate the effects of the contact grid dimensions on the cell performances compared to simulation predictions. Results of characterizations for this series of experiments are presented and compared with simulation results in regards to the variation of the width and pitch of openings.

2.2. Electrical characterization details

The experimental cells were characterized by current density-voltage (*J-V*) measurements in the dark conditions and under illumination. The dark *J-V* measurements were performed at UCLouvain with the PM8PS probe station in the four wires configuration at room temperature while the PV parameters were extracted from the *J-V* curves under AM1.5 illumination conditions at each fabrication partner site. In order to understand the obtained PV performances a special attention has been paid to the precise analysis of the dark *J-V* characteristic for the different cells from experiments and simulations.

The analytical two-diode model of a PV cell was used to extract the electrical parameters of experimental devices from the *J-V* curves in the dark. Figure 1 shows the equivalent electrical circuit for the two-diode model of a PV cell (fig. 1a) and the reduced model developed in this study with ATLAS without shunt resistance (fig. 1b) but with contact resistance used to emulate the series resistance.

Diode 1 (D_1) represents the diffusion current related to the main PN junction and is characterized by

its current density J_{01} and its non-ideality factor n_1. Diode 2 (D_2) represents the generation/recombination (*G/R*) currents and is characterized by its current density J_{02} and its non-ideality factor n_2.

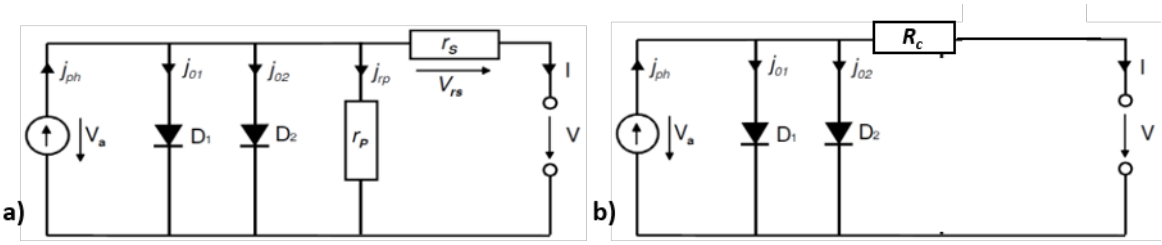

Figure 1: Equivalent electrical circuit for the two-diode model of a solar cell (a) and the reduced model for ATLAS simulations with the contact resistance (b).

The full characteristic equation of the two-diode model under illumination is presented here:

$$J(V) = J_{\mathrm{PH}} - J_{01}\left[exp\left(\frac{q(V+R_sJ)}{n_1kT}\right) - 1\right] - J_{02}\left[exp\left(\frac{q(V+R_sJ)}{n_2kT}\right) - 1\right] - \frac{V+R_sJ}{R_{\mathrm{sh}}} \quad (1)$$

where *V* is the applied voltage, *J* is the measured output current density and J_{PH} is the incident photocurrent density. *q* is the charge of the electron, *k* the Boltzmann constant and *T* the temperature.

In this model, each diode is analyzed at corresponding bias regions to discriminate the different contributions to the total current density. The *G/R* and the diffusion currents in CIGS PV cells may not be initially considered as completely separated since the non-ideality factors are indeed quite different from those ideally found in silicon cells. Nevertheless, their different contributions to the total dark current of the cell can be clearly distinguished in the *J-V* curves; while, when varying the simulation parameters, the simulations confirm the dominance of G*/R* phenomena (D_2) in reverse and low-voltage forward operation or of the diffusion (D_1) at higher voltage in forward conditions. The last term in eq.1 represents the shunt leakage current density (J_{sh}) investigated in reverse bias region [34]. It is obvious, but worth reminding, that one should be careful about the appropriate range of voltage selected for the determination of J_{02} to discriminate the effect of the shunt. It is recommended to extract R_{sh} at the minimum of *dJ/dV* to avoid underestimating J_{02} as it is discussed in [35].

This methodology has been applied for the determination of the dark electrical parameters of the experimental cells in this study. This is highly necessary in this work due to the ATLAS limitation (i.e. no R_{sh}). With this approach, our modelling results fit the experimental trends rather well and are coherent with the PV parameters extracted under illumination as discussed hereafter.

2.3. Modelling details

The modelling methodology has been built at Université catholique de Louvain (UCLouvain) with the contribution of several partners collaborating within ARCIGS-M. 2D simulations were performed using Silvaco ATLAS 2D with Deckbuild 4.6.2.R interface under room temperature, the dark and AM1.5 illumination conditions.

The global model structure used for ATLAS 2D simulations of UT-CIGS solar cells is presented in figure 2 and consists of a p-type CIGS layer of 500 nm thickness as absorber, an n-type CdS of 50 nm thickness

as buffer layer, 100 nm of i-ZnO and 300 nm of Al-doped ZnO as transparent conductive oxide layers. Molybdenum (Mo) and aluminum (Al)/nickel (Ni) were used as rear and front contact electrodes respectively. A 25 nm thin layer of Al_2O_3 with openings has been introducted at the Mo/CIGS interface as passivation layer containing a negative fixed charge density (*Qf)* in cm^{-2} and an interface traps density (*D*it) in cm^{-2}/eV. To approach the experiment as accuratly as possible, the electrical properties of the $MoSe_2$ layer, formed during the CIGS process, has been considered at the (Mo,$MoSe_2$)/CIGS interfaces (see fig.2). A work function value of 5.65 eV was used for (Mo,$MoSe_2$), forming an ohmic contact with CIGS [36], while 4.9 eV was used for Mo at Mo/Al_2O_3/CIGS interface [37]. For simplification, we will mention Mo/CIGS instead of (Mo,$MoSe_2$)/CIGS for the rest of the text. The work function value of 4.7 eV was used at the front Al/Ni alloy front metal according to litterature [38].

The input parameters used for simulations of the different layers can be found in the table 1 according to our previous work [32] and value from literature.

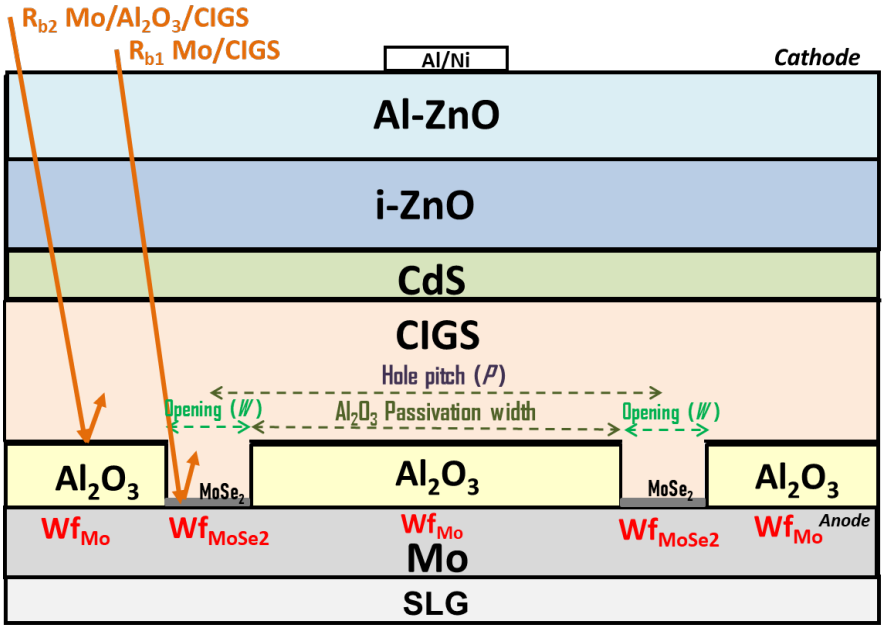

Figure 2: ATLAS 2D ARCIGS-M structure model of Al_2O_3-rear-passivated UT-CIGS cell with openings width (W) and hole pitch (P) including back reflection coeficients (R_{b1}, R_{b2}).

Beside electrical parameters integrated in ATLAS, an external optical semi-coherent model was used with the Sun*Shine* simulation tool by Ljubljana university to support accurate determination of realistic optical properties of UT-CIGS PV cell [39]. This provided some optical parameters to embed in ATLAS model such as back reflectance coefficients (R_{b1}, R_{b2}) corresponding to the optical reflection coefficients at the rear Al_2O_3 interface (R_{b2}) or back Mo contact (R_{b1}) into the CIGS (see fig. 2). These constant values were determined iteratively, by matching the absorptance curves of the CIGS layer obtained with detailed simulations of the entire cell structure using wavelength dependent reflectance spectra and simplified simulations using an average R_b value. Values of 20 % and 45 % have been obtained for R_{b1} and R_{b2} respectively in agreement with [22]. Other optical parameters such as complex refractive n, k indices of included layers have been provided from optical simulations and literature [39, 40] in order to genuinely represent light behaviour in the model.

From sensitivity analyses, the key material parameters of the passivation layers in this model are the negative charge density (*Q*f) and the interface trap density (*D*it). The *Q*f density defines the amount of fixed negative charge introduced by the Al_2O_3 passivation layer which, in turn, influences the electron and hole densities close to the rear Mo/CIGS interface by electric field effect; they are implemented in the model as negative values where the sign represent the type of charges. *D*it defines the amount of electrons/holes traps created at the interface due to the presence of the passivation layer that can trap and recombine the photogenerated carriers.

Table 1: Baseline layer parameters for the ATLAS 2D model

	CIGS	CdS	i:ZnO	Al:ZnO
Thickness (nm)	500	50	100	300
Band gap (eV)	1.15	2.4	3.3	3.3
Electron affinity (eV)	4.5	4.45	4.55	4.55
Relative Permitivity	13.6	10	9	9
Conduction band Density of state (cm^{-3})	3.1×10^{18}	1.3×10^{18}	3.1×10^{18}	3.1×10^{18}
Valence Band Density of state (cm^{-3})	1.8×10^{19}	9.1×10^{18}	1.8×10^{19}	1.8×10^{19}
Electron thermal velocity (cm/s)	3.9×10^{7}	3.1×10^{7}	2.4×10^{7}	2.4×10^{7}
Hole thermal velocity (cm/s)	1.4×10^{7}	1.6×10^{7}	1.3×10^{7}	1.3×10^{7}
Electron mobility ($cm^2/(V\cdot s)$)	100	72	100	100
Hole mobility ($cm^2/(V\cdot s)$)	12.5	20	31	3
Carrier concentration (cm^{-3})	3.0×10^{16}	5.0×10^{17}	1.0×10^{17}	5.0×10^{18}
	Bulk defect parameters			
Density of defects (cm^{-3})	1.0×10^{14}	1.0×10^{16}	1.0×10^{16}	1.0×10^{16}
Electron capture cross section (cm^2)	1.0×10^{-15}	1.0×10^{-15}	1.0×10^{-15}	1.0×10^{-15}
Hole capture cross section (cm^2)	1.0×10^{-11}	1.0×10^{-13}	5.0×10^{-13}	5.0×10^{-13}
	Rear contact		Front contact	
Work function (eV)	4.9 (Mo); 5.65 ($MoSe_2$)		4.7 (Al/Ni)	
Surface Recombination Velocity (SRV)of electrons (cm/s)	10^7 (Ref.) and 10^2 (Pass.)		10^7	
Surface Recombination Velocity (SRV) of holes (cm/s)	10^7 (Ref.) and 10^2 (Pass.)		10^7	
Resistances ($\Omega.cm^2$)	*R*s, $Rc_{Mo/CIGS}$		*R*sh not implemented	

Previous experiments estimated the absolute value of *Q*f density at the Al_2O_3/CIGS passivated interface in the range of 10^{12} cm^{-2} and the *D*it in the range of 10^{11} cm^{-2} eV^{-1} [32, 10]. The effect of the *D*it is introduced in this model through the surface velocity recombination (SRV) according to the following formula [41]:

$$SRV = \frac{U_s}{\Delta n} \qquad \text{with: } Us \cong \frac{(n_s p_s - n_i^2) * q^{-1} v_{th} D_{it}}{\frac{n_s}{\sigma p} + \frac{p_s}{\sigma n}} \qquad (2)$$

where n_s and p_s are the surface densities of electrons and holes respectively, σ_n, σ_p are the cross-sections of electrons and holes respectively, v_{th} being the thermal velocity, U_S is the recombination rate and Δn is the excess carrier density. The SRV value of 10^2 cm/s considered in this work at the

Al_2O_3/CIGS interface for the passivated cells is a conservative value based on the fitting with experimental results.

This model intrinsically simulates the behavior of the cell assuming an infinite shunt resistance (R_{sh}) with no additional external series resistance (R_s). However, a contact resistance (R_c) in Ω.cm^2 can be specified at the Metal/Semiconductor interface. We use it here to directly emulate the experimental R_s for reference cells, while for passivated cells, we convert R_s in an equivalent R_c at the Mo/CIGS interface within the contact holes according to the following equation:

$$R_C = R_s * \frac{W}{P} \quad (3)$$

The reason for this approximation is that, for the reference cell, the Mo/CIGS interface covers the whole cell area, while for the passivated cells, that contact interface appears only within the openings that cover a *W/P* ratio of the total cell area. The experimental R_s value then leads to an approximated contact resistance R_c at the Mo/CIGS rear interface that represents the losses due to series resistance depending on the opening size. Such approach limits the approximation related to the 2D modelling compared to the 3D reality and reproduces the experimental trends as demonstrated below.

3. Results and discussions:

3.1. Characterizations versus simulations: effects of Al_2O_3-rear-passivation on UT-CIGS cells

In this section, based on the series of experimental cells from INL compared with simulations, we present and discuss the effects of the passivation on the *J-V* characteristic in the dark and their correlations with the PV parameters obtained under illumination. Next, the obtained results are compared with simulation results for different parameters of the passivation layer.

Figure 3 presents the *J-V* curves of reference and passivated cells measured in the dark at room temperature. The dark electrical parameters extracted from figure 3 and the PV parameters extracted under illumination are listed in the table 2 [33].

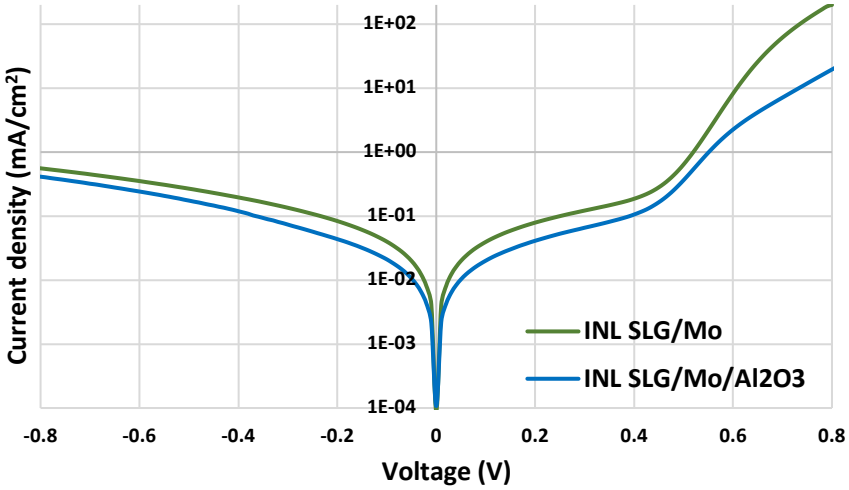

Figure 3: Dark J-V curves in logarithm scale for INL reference (SLG/Mo) and Al_2O_3-rear-passivated (SLG/Mo/Al2O3) UT-CIGS cells.

We observe that the *G/R* current density J_{02} as well as the diffusion current density J_{01} in the dark are reduced for the passivated cell compared to the reference, meaning a decrease of the diffusion and a decrease of the *G/R* phenomenon due to the introduction of the passivation layer. The decrease of the recombination results in a better collection of the photo-generated electron/hole pairs under illumination that leads to an increase of the *J*sc, while a decrease of the diffusion current leads to better transport properties at the main CIGS/CdS junction that improves the *V*oc value above the reference one. Thanks to the Al_2O_3-rear-passivation, in this experiment, an increase in absolute value of *J*sc by about 2.88 mA/cm^2 and an increase in absolute value of *V*oc by 36 mV is observed. We observed a reduction of the *FF* for passivated compared to reference due to an increase of the series resistance compensated by the increase of the product *J*sc**V*oc that leads to an increase of absolute value of the *Eff* by 1.4 %.

Table 2: Electrical parameters for INL reference and passivated UT-CIGS cells extracted in the dark and under illumination.

Electrical parameters	J_{01} (mA/cm^2)	J_{02} (mA/cm^2)	R_s (Ω.cm^2)	R_{sh} (Ω.cm^2)	*J*sc (mA/cm^2)	*V*oc (mV)	*FF* (%)	*Eff* (%)
SLG/Mo	7.13×10^{-5}	2.06×10^{-2}	0.69	$2.11\times10^{+3}$	21.4	573.1	66.5	8.15
SLG/Mo/Al_2O_3	4.20×10^{-5}	6.68×10^{-3}	1.84	$3.86\times10^{+3}$	24.3	609.1	64.7	9.50

This series of experiments have been reproduced by simulation with our model for different properties of the Al_2O_3 passivation layer on UT-CIGS PV cells. Three specific *Q*f values have been chosen (-8×10^{12} cm^{-2}, -5×10^{12} cm^{-2} and -1×10^{12} cm^{-2}) in the range of experimental values for the passivated cells in order to feel the sensitivity of the performances due to the variation of the oxide charge density at the passivation interface. The SRV has first been kept constant at 10^2 cm/s and then varied from 10^2 cm/s to 10^7 cm/s at the Al_2O_3/CIGS passivated interface, while the value of 10^7 cm/s was maintained at the Mo/CIGS interface. The opening width *W* was kept constant at 200 nm for a 2 µm pitch like in experiment. Our approximation model of resistances described in section 2.3 has been applied to the experimental resistance values that gives a *R*c of 0.69 Ω.cm^2 for the reference cell and 0.18 Ω.cm^2 (i.e. 1.81*0.2/2) for the passivated cell respectively.

We plotted in figure 4 the *J-V* curves in the dark resulting from the simulation of the passivated cells with the three different *Q*f values compared with the reference cell; the simulated PV parameters are summarized in table 3. Note that the simulated dark current density of figure 3 does not consider the contribution of the shunt current density. In fact, the leakage current density in the dark could be increased due to a very high shunt current within the cell (i.e. *R*sh below 1×10^4 Ω.cm^2) and cause the S-shape observed in experimental INL dark *J-V* curves (fig.3). However, based on simulations, its degradation effect on the PV performances under illumination, especially on the *FF*, is observed for very low shunt resistance value only (below 1×10^3 Ω.cm^2).

We observe in fig.4 that, when the absolute value of the *Q*f density is high enough (5×10^{12} cm^{-2} or 8×10^{12} cm^{-2}), the dark current density is reduced both in forward and reverse operations as observed in experiments. The reduction of the dark current in reverse and at low voltage (leakage current) induces a reduction of the J_{02} current density related to the recombination phenomena, this contributes to the improvement of the *J*sc observed under illumination of about 1.4 - 1.5 mA/cm^2 in the table 3. The reduction of the diffusion current density in the dark J_{01} linked to the main junction is

related to the passivation-induced rear electrical field and induces an improvement of the *V*oc, here about 40 mV. The link between the J_{01} and the *V*oc can be approximated by the following first-order well-known formula [42]:

$$Voc = \frac{nkT}{q} ln\left[\frac{J_{Ph}}{J_0} + 1\right] \quad (4)$$

where *n* is the non-ideality factor, *k* the Boltzmann constant, *q* the charge of the electron, J_{Ph} the photocurrent generated by incident light and J_0 the diffusion current density of the cell.

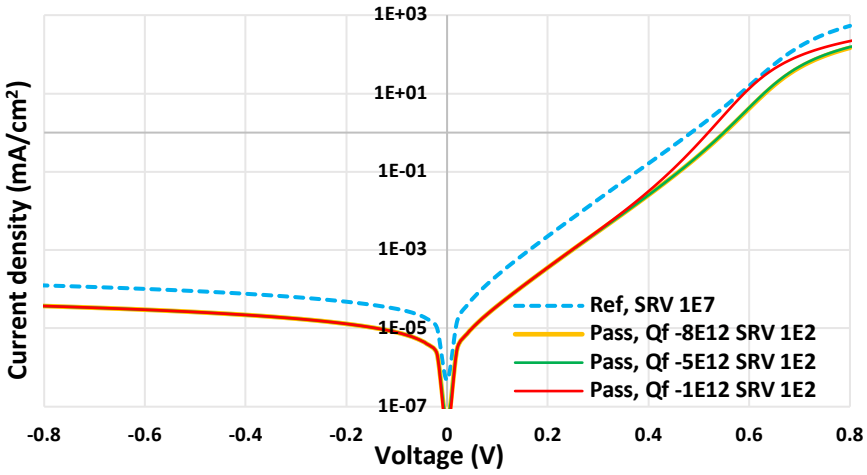

Figure 4: Simulated J-V curves in the dark for reference cells (blue dashes) with an SRV of 1×10^{7} cm.s^{-1} *and passivated cells with an SRV of* 1×10^{2} cm.s^{-1} *with three different Qf values of* -8×10^{12} cm^{-2} *(yellow lines),* -5×10^{12} cm^{-2} *(green lines) and* -1×10^{12} cm^{-2} *(red lines).*

Table 3. Simulated PV parameters of reference and passivated cells for three different Qf values

	Reference	Passivated *Q*f = -8×10^{12}	Passivated *Q*f = -5×10^{12}	Passivated *Q*f = -1×10^{12}
*J*sc (mA/cm^2)	26.62	28.13	28.04	26.79
*V*oc (mV)	659.79	700.74	695.05	661.58
FF (%)	76.15	72.75	72.87	71.54
Eff (%)	13.38	14.34	14.20	12.68

Reducing the absolute value of *Q*f of the passivated cell from 8×10^{12} cm^{-2} to 5×10^{12} cm^{-2} leads to a slight increase of the dark current, especially visible at high voltage around J_{01} that causes a slight reduction of the *V*oc and the *J*sc under illumination (by about 5 mV and 0.1 mA/cm^2) while they still remain significantly above the reference.

When the absolute value of *Q*f of the passivated cell is reduced down to 1×10^{12} cm^{-2}, a significant increase of the diffusion current is observed that reduces the *V*oc according to equation (4). The G/*R* forward and reverse current densities show a slight increase that supposes an increase of the recombination which reduces the *J*sc close to the reference. We notice a significant decrease of the *FF* that reduce the efficiency of the cell below the reference. The increase of the diffusion current in the dark is surprising as the Al_2O_3 layer is introduced to passivate the rear Mo/CIGS interface and improve its electrical properties. Particularly, its detrimental effect on the J_{01} of the main junction,

when the *Q*f density is very low was not reported or investigated before. Our simulation results show that to the first order, it is related to an inversion of the electrical field, due to electrons instead of holes, at the rear interface of the passivated CIGS cells for too low oxide charges *Q*f.

The preceding modeling analysis is limited to a specific case of low recombination velocity at Al_2O_3/CIGS interface. In experiments, according to the *Q*f density introduced by the oxide layer, the passivation mechanism reduces the recombination by attracting holes at the oxide/semiconductor interface and repelling the electrons out of it. This has a significant impact on the cell performances as shown in the following figure 5 where we clearly see that, when reducing the recombination velocity, the efficiency is improved. However, simulations demonstrate that a large value of negative *Q*f is more important and efficient with regards to electrical field passivation, than a reduction of *D*it or SRV (hence improving chemical passivation) [43, 44].

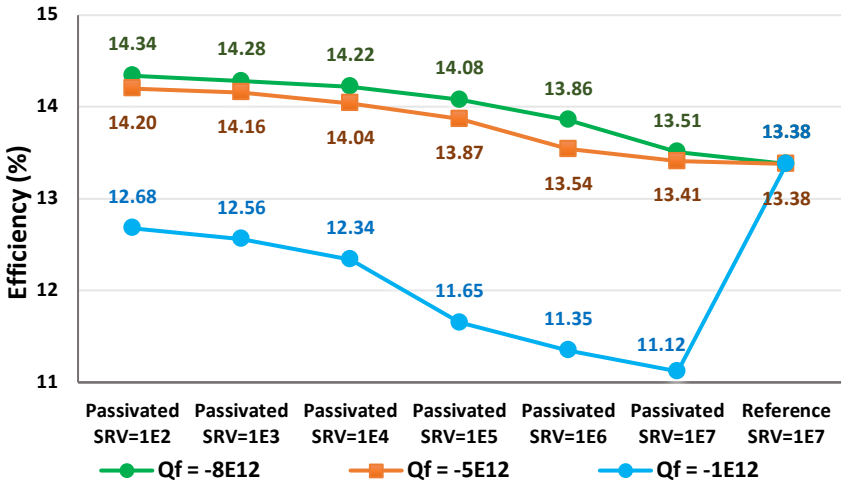

Figure 5: Efficiency of reference cell with SRV = 1×10^7 cm/s *and passivated cells with different SRV values from* 1×10^7 to 1×10^2 cm/s *and different Qf densities (*-8×10^{12} cm^{-2}, -5×10^{12} cm^{-2}, -1×10^{12} cm^{-2}*).*

As will be discussed hereafter, this simulation results could help to understand some experimental results where the cell performances are either improved or reduced after Al_2O_3-rear-passivation. This latest can be attributed to a poor passivation quality, or to a high contact resistance in other cases as will be discussed in the next section. Therefore, an increase of the diffusion current J_{01} in the dark and a low *V*oc under illumination, respectively from one passivated cell to another, can be used to characterize poor passivation (i.e. insufficiently negative *Q*f) experimentally. Further investigations are ongoing to better understand these intricate effects of the Al_2O_3-rear-passivation layer especially on UT-CIGS solar cells.

3.2. Optimization of openings width of Al_2O_3-rear-passivated UT-CIGS cells

The geometry, the size and the distribution of the contact holes have been found to be very important for the performance of the passivated cells. As our 2D model is limited in exact resistances definition, we will therefore present the next results in terms of gains on PV parameters of passivated cells compared to reference ones. Gains on PV-parameters (Δ*J*sc, Δ*V*oc, Δ*FF*, Δ*Eff*) are here the difference between the absolute values of a parameter after passivation and of its value for the reference cell. Therefore, a gain equal to 0 corresponds to the value of the parameter for the reference cell. We

present in figure 6 the gains on the four PV parameters for a passivated cell with different opening width (*W)* at a fixed pitch (*P* = 0.5 µm) with and without contact resistance at the Mo/CIGS interface within the openings. We considered here passivated cells with the two specific *Q*f values -8×10^{12} cm^{-2} and -1×10^{12} cm^{-2} at the Al_2O_3/CIGS interface for a fixed SRV of 1×10^{2} $cm.s^{-1}$.

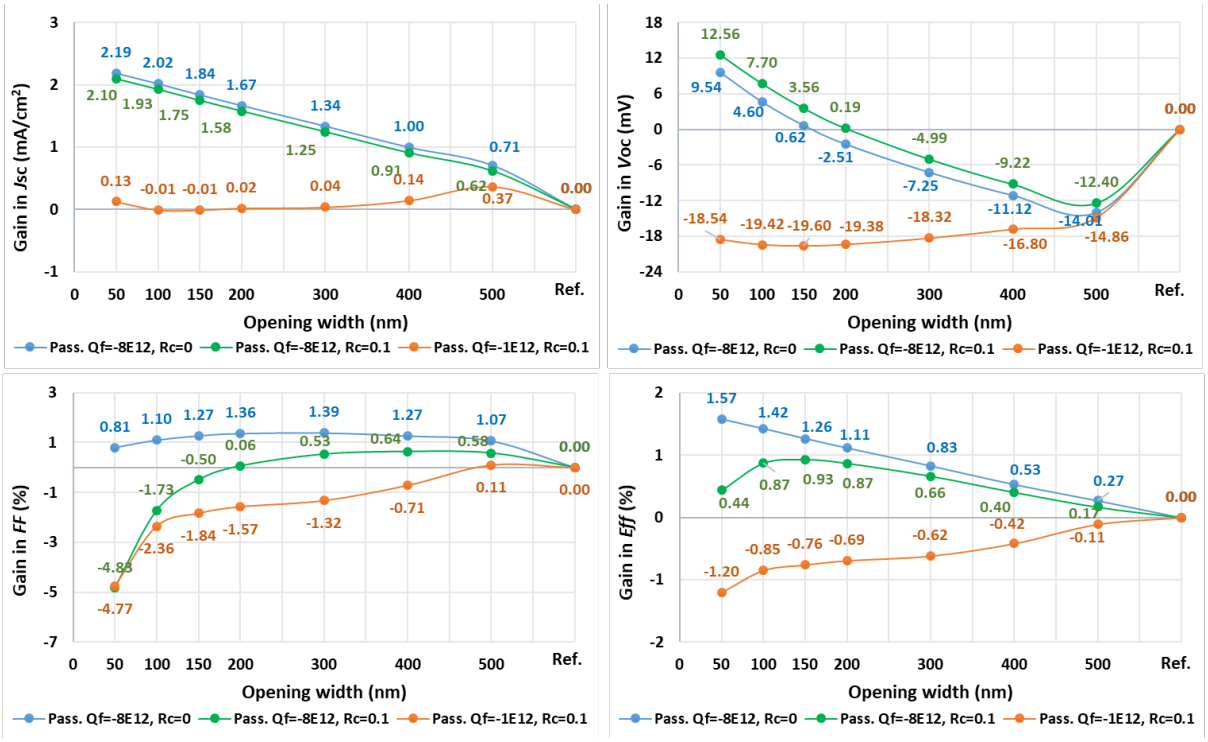

Figure 6: Gains on absolute values of PV-parameters for passivated UT-CIGS cells for different opening widths at fixed pitch of 0.5 µm *with and without* R*c and for two Q*f *densities: Q*f = -8×10^{12} cm^{-2} *with* R*c* = 0 Ω.cm^2 *(blue curves), Q*f = -8×10^{12} cm^{-2} *with* R*c* = 0.1 Ω.cm^2 *(green curves), and Q*f = -1×10^{12} cm^{-2} *with* R*c* = 0.1 Ω.cm^2 *(red curves).*

We observe that, when the negative *Q*f density is high enough (8×10^{12} cm^{-2}), the *J*sc of the passivated cells are improved compared to reference as discussed before. However, we find that its value decreases when increasing the opening width values. We can attribute this decrease of *J*sc to the increase of the effective recombination rate at the Mo/CIGS interface that increases when increasing the openings and thereby the contact area. *V*oc decreases when increasing the opening widths due to the reduction of the passivation effect on the diffusion current when decreasing the passivation area (increase of opening width). Its values are higher than the reference only for a certain range of opening width where the passivation area is large compared to the contact hole area and the gains are limited by the value of the contact resistance. With *R*c taken into consideration (green curve in fig.6), the fill-factor is degraded below the reference for low opening widths because of an increase of the series resistance already predicted by simulations and observed experimentally. However, when the passivation area become larger compared to the contact hole area, the *FF* of the passivated cell is improved compared to reference.

The resulting efficiency of the cell, which is a combination of the previous mentioned parameters, first increases from small openings where passivation has a higher effect on the performances, passes by an optimum value and then decreases when the size of openings are further increased due to the

reduction of the passivation area that leads to an increase of the recombination at the Mo/CIGS interface.

All those trends and positive effects of passivation are negated when the absolute value of *Q*f is reduced down to 1×10^{12} cm^{-2}. Simulations show that, in this case, electrons present at the Al_2O_3/CIGS interface recombine with photogenerated holes, degrading the PV parameters of the cells, finally leading to worse performance than the reference cell.

We point out here the presence of an optimum in efficiency for passivated cells at an opening width in the range of 100 - 150 nm for a fixed hole pitch of 0.5 µm that correspond to an opening width to pitch ratio between 0.2 and 0.3 and the sensitivity of the performance to a variation of the opening width around that optimum, for non-zero contact resistance. This can help to explain the small differences of performances observed for different cells on a same sample or from one process to another, due to variation of *W*, *Q*f and *R*c, apart from other material and defect state differences. This novel result about optimal *W/P* ratio shows the crucial importance to have and to control a suitable design of the contact openings as well as a lower contact resistance for best performances in Al_2O_3-rear-passivated UT-CIGS cells.

3.3. Optimization of holes pitch size of Al_2O_3-rear-passivated UT-CIGS cells

In this section, we extended the study to different pitch distances to clear out a general trend on the optimal configuration with regards to *W* and *P*. The aim was to investigate the possibility to increase the size of the openings and the pitch to make it less challenging during fabrication of the rear contact grid. We simulated the passivated cell for different opening widths and different pitches. We increased the openings width from 100 nm to 3000 nm considering different pitches *P* from 1 µm to 4 µm with typical density of negative charges *Q*f = -8×10^{12} cm^2 and *R*c = 0.1 Ω.cm^2. The impact on the PV performances has been simulated and compared to reference cells. Simulation results, summarized in figure 7, show the different gains in *J*sc, *V*oc, *FF* and *Eff* compared to reference versus opening widths for each pitch size.

At constant *W*, we observe an increase of the gains Δ*J*sc and Δ*V*oc that tend to saturate at high pitches for small openings, when we increase the pitch and therefore the passivated area. On the other hand, the gain Δ*FF* decreases at constant *W* as we reduce the opening width to pitch ratio (*W/P*) and increase the series resistance implemented as contact resistance in this study. As a result, the optimum gain in efficiency Δ*Eff*, when the material parameters and the specific contact resistance are kept constant, increases towards larger *W* for larger *P* values. For example, increasing the pitch up to 2 - 4 µm is not detrimental for the cell performances compared to a cell with 1 µm pitch as long as we increase the optimum *W* up to 400 - 800 nm. This result is very important for the cell design and provides direction towards next processes as experimentally, a large opening grid is less difficult and less costly to produce.

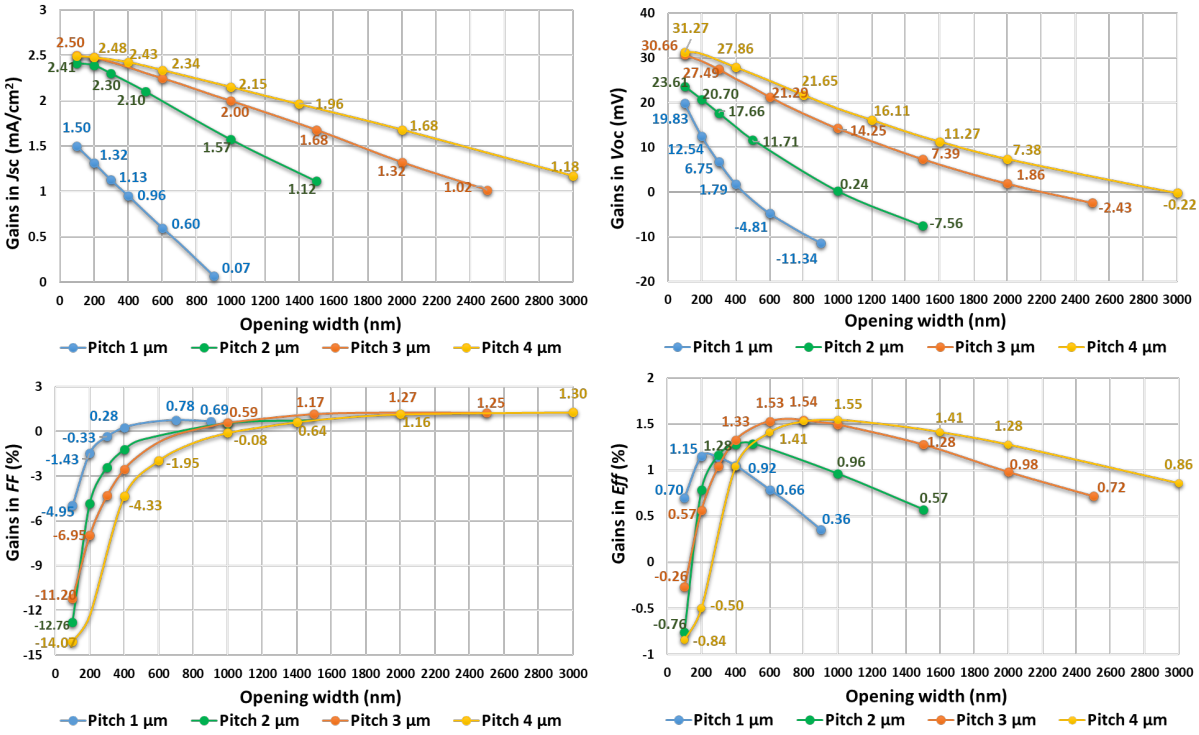

Figure 7: Gains on absolute values of PV-parameters for passivated cells compared to reference for hole pitches of 1 µm *(blue curve),* 2 µm *(green curve)* 3 µm *(orange curve) and* 4 µm *(yellow curve) as a function of different opening widths at fixed Rc.*

We predict in this study an increase of the efficiency by about 1.4 - 1.5 % in absolute value thanks to passivation which agrees closely to the gains generally demonstrated by experiments with an opening to pitch (*W*/*P*) ratio around 0.2 for each cell configuration that is close to our model test structure. However, during the fabrication processes, many phenomena can occur leading to a variation of material and interface/bulk defect properties in the cells. These different possible variations can induce either a positive or a negative effect on the PV performances of the cell.

It should be noted that around the optimum predicted by this study for *W*/*P* ratios around 0.2, (i) for *W*/*P* ratios > 0.4 - 0.5, a loss of *V*oc can be observed when compared to the reference, though the rear interface is well passivated and the *J*sc is higher as well as the efficiency, or (ii) for *W*/*P* < 0.1, large gains in *J*sc and in *V*oc are negated in terms of efficiency by a large loss on *FF* due to the high series resistance.

The series of reference and Al_2O_3-rear-passivated cells from CNRS and Solibro with different hole pitches at fixed opening width will serve as experimental study case. The values of hole pitches for the passivated cells are *P* = 1 µm, 2 µm, 3 µm and 4 µm with an average measured opening width *W* of ± 300 nm. The cells have been characterized under AM1.5 illumination and the measured average PV parameters as well as the average series and shunt resistances of all devices per sample types are summarized in the table 4.

Table 4: Average output PV-parameters and resistance values of reference and passivated cells from CRNS/Solibro series with different pitch sizes (P = 1, 2, 3 and 4 µm) at constant opening W = 300 nm.

	Pitch (µm)	*W/P* ratio	*R*s ($\Omega.cm^2$)	*R*sh ($\Omega.cm^2$)	*J*sc (mA/cm^2)	*V*oc (mV)	*FF* (%)	*Eff* (%)
Reference	-	-	0.13	455.20	20.02	663.5	71.85	10.94
Passivated	1	0.30	1.94	473.40	21.56	682.0	64.69	10.34
	2	0.15	0.40	365.42	22.85	677.6	67.85	11.48
	3	0.10	1.69	547.95	21.45	681.7	58.29	9.26
	4	0.08	2.53	831.95	22.05	676.1	61.11	9.81

We observe that, thanks to the passivation, both the *J*sc and the *V*oc of the passivated cells are higher than the reference, with gains of about 1.5 to 2.8 mA/cm^2 and 12 to 19 mV respectively. On the contrary, the *FF* values of passivated cells are strongly degraded, as expected from the higher series resistance induced by localized contacts through small holes. Depending on the different dimensions of the opening grid (*W*/*P* ratio) and the resistance values, the efficiencies of passivated cells are either improved or reduced as compared to the reference cell when increasing *P* from 1 µm to 4 µm, with a best efficiency achieved for a pitch *P* = 2 µm. The latter case that corresponds to a *W/P* ratio of 0.15, agrees with simulation predictions of the optimum around 0.2. When increasing the pitch, the *W*/*P* ratio decreases and the gains in *J*sc and in *V*oc are negated by the large loss on *FF* due to resistances as predicted by simulations. These results are close to our simulation trends but show some variations in performance between the real devices and the theoretical simulation models probably due to fabrication processes variabilities.

It has to be noted that in real cells, the back-grid openings are organized in a very regular matrix in all directions. Therefore, a series of regular openings in the third direction will then behave like a line contact with a different series resistance and passivation area than the 2D model that assumes homogeneous properties in the third dimension. However, as we fit the empirical contact resistance *R*c in the 2D model from the experimental *R*s value and the opening width to pitch ratio, the specific *R*c value obtained in a 3D model would be different, but the equivalent *R*s would be the same. With regards to the effect of the passivation area, it should be noted that what matters is the lateral collection of photogenerated carriers which depends on the diffusion length compared to the distance to the contact. In a regular 3D model, in the worst case, that distance can only become 40% larger than the half-pitch considered in the 2D model. That could probably result in different absolute values for optimal *W* and *P* parameters, but the general trends should remain the same and keep the message of this work, i.e. that the optimal *W/P* is around 0.15 - 0.20, supported by both simulations and experiments. For example, *G. Sozzi* in [45] reported on a 3D simulation work, an optimal opening width of 400 nm for a 2 µm pitch and *R*c of 10^{-4} $\Omega.cm^2$ for absolute value of $Q_f \geq 5\times10^{12}$ cm^{-2} on a 3 µm CIGS PV cell that fit with our results (*W/P* = 0.2). However, compared to their work, our simulations have targeted ultra-thin CIGS cells, discussed in-depth the effects of the passivation properties on the dark current and on the different PV parameters under illumination, and furthermore achieved an optimization of the full back grid (*W* and *P*) dimensions supported by experimental results.

Conclusion

The key of success of the proposed modelling of the rear contact grid in passivated UT-CIGS cells is the correlation of the general trends with the experimental results while limited for the absolute values by the exact material properties especially the bulk and interface defect states and the resistances definition. We discussed the optimization of the Al_2O_3-rear-passivated cell according to the dimensions of the contact openings in the passivation layer and its influence on the electrical behavior in the dark current and on the PV-parameters of the cell under illumination. The latter mostly depend on passivation quality (i.e. density of negative fixed oxide charges) and contact resistance. It comes out that apart from the improvement due to the material qualities, especially for the oxide passivation layer, it is crucial to optimize the dimensions of the openings to improve the transport with less resistance effects, i.e. keep a good *FF*, while maintaining excellent rear passivation. Experimental results sometimes show different, even opposed or detrimental effects of rear passivation on cell performances under illumination. Our simulations relate these contradictory observations to the interplay between the area and quality of the passivation layer on one hand and the size, density and contact resistance of openings in this passivation layer on the other hand. Variations of these parameters around their optimum values can lead to positive or negative trends on the cell performances. Subsequently, characterizing these performances under illumination is not sufficient to assess the passivation quality due to the possible impact of the shunt and series resistances. Our extensive results demonstrate that the quality of the passivation can be directly related to increases of *J*sc under illumination and reduction of diffusion (J_{01}) and G/R (J_{02}) diode currents in the dark when compared to the unpassivated cells, both experimentally and by simulations. On the other hand, *V*oc under illumination is not a straightforward indicator of the quality of the passivation interface since it may become higher or smaller than the reference cell depending on the opening width to pitch ratio. This study revealed the presence of an optimum in PV performances for an opening width to pitch (W/P) ratio around 0.2 for a good passivation quality. We finally show how a suitable 2D modelling can yield additional and more accurate insights on the results of characterizations of cells and hence can guide the experiences and provide useful interpretation, direction and trends for the fabrication process.

Acknowledgements

This work is supported by the ARCIGS-M project within the European Union's Horizon 2020 research and innovation program under grant agreement No. 720887.

References

[1] J. Ramanujam, U. P. Singh, Copper Indium gallium selenide based solar cells - a review, Energy Environ. Sci., 10 (2017) 1306 - 1319

[2] B. P. Jelle, Building integrated photovoltaics: A concise description of the current state of the art and possible research pathways, Energies 9 (2016) 21.

[3] J. Goffard, A. Cattoni, F. Mollica, M. Jubault, C. Colin, J.-F. Guillemoles, D. Lincot, N. Naghavi, S. Collin, Nanostructured back mirror for ultra-thin CIGS solar cells, Proc. 31th European Photovoltaic Solar Energy Conference (2015) 1050 - 1052.

[4] N. Naghavi, F. Mollica, J. Goffard, J. Posada, A. Duchatelet, M. Jubault, F. Donsanti, A. Cattoni, S. Collin, P. P. Grand, J. J. Greffet, D. Lincot, Ultrathin Cu(In,Ga)Se_2 based solar cells, Thin Solid Films 633 (2017) 55 - 60.

[5] O. Lundberg, M. Edoff, L. Stolt, The effect of Ga-grading in CIGS thin film solar cells, Thin Solid Films 480–481 (2005) 520 - 525.

[6] S. Schleussner, U. Zimmermann, T. Wätjen, K. Leifer, M. Edoff, Effect of gallium grading in Cu(In,Ga)Se_2 solar-cell absorbers produced by multi-stage co-evaporation, Solar Energy Materials & Solar Cells 95 (2011) 721 - 726.

[7] M. Edoff, S. Schleussner, E. Wallin, O. Lundberg, Technological and economical aspects on the influence of reduced Cu(In,Ga)Se_2 thickness and Ga grading for co-evaporated Cu(In,Ga)Se_2 modules, Thin Solid Films 519 (2011) 7530 - 7533.

[8] W.-C. Chen, L. Stolt, M. Edoff, Ga/(Ga + In) grading effects on ultra-thin (UT) CIGS solar cell, Conference: IEEE-PVSC 46, Chicago, Illinois, (June 2019).

[9] R. Kotipalli, B. Vermang, V. Fjällström, M. Edoff, R. Delamare, D. Flandre, Influence of Ga/(Ga + In) grading on deep-defect states of Cu(In,Ga)Se_2 solar cells, Phys. Status Solidi RRL 9 (2015) 157 - 160.

[10] R. Kotipalli, B. Vermang, J. Joel, R. Rajkumar, M. Edoff, D. Flandre, Investigating the electronic properties of Al2O3/Cu(In, Ga)Se2 interface, AIP ADVANCES, 5 (2015) 107101.

[11] B. Vermang, V. Fjällström, J. Pettersson, P. Salomé, M. Edoff, Development of rear surface passivated Cu(In,Ga)Se_2 thin film solar cells with nano-sized local rear point contacts, Solar Energy Materials & Solar Cells 117 (2013) 505 - 511.

[12] B. Vermang, F. Rostvall, V. Fjällström, M. Edoff, Potential-induced optimization of ultra-thin rear surface passivated CIGS solar cells, Phys. Status Solidi RRL 8, (2014) 908.

[13] José M. V. Cunha, Célia Rocha, Carlos Vinhais, Paulo A. Fernandes and Pedro M. P. Salomé, Understanding the AC Equivalent Circuit Response of Ultrathin Cu(In,Ga)Se2 Solar Cells, IEEE Journal of Photovoltaics, IEEE JOURNAL OF PHOTOVOLTAICS, 9 (2019) 1442 - 1448.

[14] Sourav Bose, José M. V. Cunha, Sunil Suresh, Jessica De Wild, Tomás S. Lopes, João R. S. Barbosa, Ricardo Silva, Jérôme Borme, Paulo A. Fernandes, Bart Vermang, and Pedro M. P. Salomé, Optical Lithography Patterning of SiO2 Layers for Interface Passivation of Thin Film Solar Cells, Sol. RRL (2018) 1800212.

[15] J. M. V. Cunha, P. A. Fernandes, A. Hultqvist, J. P. Teixeira, S. Bose, B. Vermang, S. Garud, D. Buldu, J. Gaspar, M. Edoff, J. P. Leitão and P. M. P. Salomé, Insulator materials for interface passivation of Cu(In,Ga)Se2 thin films IEEE JOURNAL OF PHOTOVOLTAICS, 8 (2018) 1313 - 1319.

[16] D Ledinek, P Salomé, C Hägglund, U Zimmermann, M Edoff, Rear Contact Passivation for High Bandgap Cu(In, Ga)Se2 Solar Cells With a Flat Ga profile, IEEE Journal of Photovoltaics, 8 (2018) 864 - 870.

[17] Pedro M. P. Salomé, Bart Vermang, Rodrigo Ribeiro-Andrade, Jennifer P. Teixeira, José M. V. Cunha, Manuel J. Mendes, Sirazul Haque, Jêrome Borme, Hugo Águas, Elvira Fortunato, Rodrigo Martins, Juan C. González, Joaquim P. Leitão, Paulo A. Fernandes, Marika Edoff and Sascha Sadewasser, Passivation of Interfaces in Thin Film Solar Cells: Understanding the Effects of a Nanostructured Rear Point Contact Layer, Advanced Materials Interfaces, 5(2) (2018) https:/doi.org/10.1002/admi.201701101.

[18] B. Vermang, V. Fjällström, X. Gao, M. Edoff, Improved Rear Surface Passivation of Cu(In,Ga)Se_2 Solar Cells: A Combination of an Al_2O_3 Rear Surface Passivation Layer and Nanosized Local Rear Point Contacts, IEEE journal of photovoltaics, vol. 4, (2014) 486 - 492.

[19] B. Vermang, J. T. Wätjen, V. Fjällström, F. Rostvall, M. Edoff, R. Gunnarsson, I. Pilch, U. Helmersson, R. Kotipalli, F. Henry, D. Flandre, Highly reflective rear surface passivation design for ultra-thin Cu(In,Ga)Se_2 solar cells, Thin Solid Films 582 (2015) 300 - 303.

[20] F. Werner, M. H. Wolter, S. Siebentritt, G. Sozzi, S. D. Napoli, R. Menozzi, P. Jackson, W. Witte, R. Carron, E. Avancini, T. Paul Weiss, S. Buecheler, Alkali treatments of Cu(In,Ga)Se_2 thin-film absorbers and their impact on transport barriers, Prog Photovolt Res Appl. 26 (2018) 911 - 923.

[21] Y. Sun, S. Lin, W. Li, S. Cheng, Y. Zhang, Y. Liu, W. Liu, Review on Alkali Element Doping in Cu(In,Ga)Se_2 Thin Films and Solar Cells, Engineering 3 (2017) 452 - 459.

[22] J. Goffard, C. Colin, F. Mollica, A. Cattoni, C. Sauvan, P. Lalanne, J.-F. Guillemoles, N. Naghavi, S. Collin, Light Trapping in Ultrathin CIGS Solar Cells with Nanostructured Back Mirrors, IEEE journal of photovoltaics 7, (2017) 1433 - 1441.

[23] L. Gouillart, A. Cattoni, J. Goffard, F. Donsanti, G. Patriarche, M. Jubault, N. Naghavi, S. Collin, Development of reflective back contacts for high-efficiency ultrathin Cu(In,Ga)Se_2 solar cells, Thin Solid Films 672 (2019) 1 - 6.

[24] O. Poncelet, R. Kotipalli, B. Vermang, A. Macleod, L. A. Francis, D. Flandre, Optimization of rear reflectance in ultra-thin CIGS solar cells towards >20% efficiency, Solar Energy 146 (2017) 443 - 452.

[25] Tomás S. Lopes ; José M. V. Cunha ; Sourav Bose ; João R. S. Barbosa ; Jérôme Borme, Olivier Donzel-Gargand, Célia Rocha, Ricardo Silva, Adam Hultqvist, Wei-Chao Chen, Ana G. Silva, Paulo A. Fernandes, Pedro M. P. Salomé, Rear Optical Reflection and Passivation Using a Nanopatterned Metal/Dielectric Structure in Thin-Film Solar Cells, IEEE Journal of Photovoltaics, 9(5) (2019) 1421 - 1427.

[26] José M. V. Cunha, Tomás S. Lopes, Sourav Bose, Adam Hultqvist, Wei-Chao Chen, Olivier Donzel-Gargand, Rodrigo M. Ribeiro, Antonio J. N. Oliveira, Marika Edoff, Paulo A. Fernandes and Pedro M. P. Salomé, Decoupling of Optical and Electrical Properties of Rear Contact CIGS Solar Cells, accepted in IEEE Journal of Photovoltaics, 2019, DOI:10.1109/JPHOTOV.2019.2933357.

[27] M. Schmid, Review on light management by nanostructures in chalcopyrite solar cells, Semicond. Sci. Technol. 32 (2017) 043003.

[28] M. Mostefaoui, H. Mazari, S. Khelifi, A. Bouraiou, R. Daboua, Simulation of High Efficiency CIGS solar cells with SCAPS-1D software, Energy Procedia 74 (2015) 736 - 744.

[29] X. Shang, Z. Wang, M. Li, L. Zhang, J. Fang, J. Tai, Y. He, A numerical simulation study of $CuInS_2$ solar cells, Thin Solid Films 550 (2014) 649 - 653.

[30] Md. B. Hosen, A. N. Bahar, Md. K. Ali, Md. Asaduzzaman, Modelling and performance analysis dataset of a CIGS solar cell with ZnS buffer layer, Data in Brief 14 (2017) 246 - 250.

[31] H. Heriche, Z. Rouabah, N. Bouarissa, New ultra-thin CIGS structure solar cells using SCAPS simulation program, International journal of hydrogen energy 42 (2017) 9524-9532.

[32] R. Kotipalli, O. Poncelet, G. Li, Y. Zeng, L. A. Francis, B. Vermang, D. Flandre, Addressing the impact of rear surface passivation mechanisms on ultra-thin $Cu(In,Ga)Se_2$ solar cell performances using SCAPS 1-D model, Solar Energy 157 (2017) 603–613.

[33] S. Bose, J. M. V. Cunha, J. Borme, W. C. Chen, N. S. Nilsson, J. P. Teixeira, J. Gaspar, J. P. Leitão, M. Edoff, P. A. Fernandes, and P.M.P. Salomé, A morphological and electronic study of ultrathin rear passivated $Cu(In,Ga)Se_2$ solar cells, Thin Solid films 671 (2019) 77-84.

[34] S. Dongaonkar, J. D. Servaites, G. M. Ford, S. Loser, J. Moore, R. M. Gelfand, H. Mohseni, H. W. Hillhouse, R. Agrawal, M. A. Ratner, T. J. Marks, M. S. Lundstrom, M. A. Alam, Universality of non-Ohmic shunt leakage in thin-film solar cells, JOURNAL OF APPLIED PHYSICS 108 (2010) 124509.

[35] S. S. Hegedus, W. N. Shafarman, Thin-film solar cells: device measurements and analysis, Progress in Photovoltaics: Research and Applications 2004, 12, 155.

[36] Keszler, D. A.; Wager, J. F. Novel Materials Development for Polycrystalline Thin-Film Solar Cells: Final Subcontract Report, 26 July 2004-15 June 2008; Office of Scientific and Technical Information (OSTI), (2008) 1-16.

[37] S. Berge, P. O. Gartland, B. J. Slagsvold, Photoelectric work function of a molybdenum single crystal for the (100), (110), (111), (112), (114), and (332) faces, Surf. Sci., 43 (1974) 275-292.

[38] T. Matsukawa, C. Yasumuro, H. Yamauchi, S. Kanemaru, M. Masahara, K. Endo, E. Suzuki, J. Itoh, Work function control of Al-Ni alloy for metal gate application, Extended Abstracts of the 2004 International Conference on Solid State Devices and Materials, Tokyo, 2004, - 464 - P3-10 pp. 464-465

[39] J. Krc, M. Sever, A. Campa, Z. Lokar, B. Lipovsek, M. Topic, Optical confinement in chalcopyrite based solar cells, Thin Solid Films 633 (2017) 193–201.

[40] M. Kovacic, J. Krc, B. Lipovsek, W.-C. Chen, M. Edoff, P.J. Bolt, J. van Deelen, M. Zhukova, J. Lontchi, D. Flandre, P. Salomé, M. Topic, Light management design in ultra-thin chalcopyrite photovoltaic devices by employing optical modelling, Solar Energy Materials and Solar Cells 200 (2019) 109933.

[41] R. B. M. Girisch, R. P. Mertens, and R. F. De Keersmaecker, Determination of Si-SiO2 interface recombination parameters using a gate-controlled point- junction diode under illumination, IEEE Transactions on Electron Devices, 35 (1988) 203-222.

[42] J. Yao, T. Kirchartz, M. S. Vezie, M. A. Faist, W. Gong, Z. He, H. Wu, J. Troughton, T. Watson, D. Bryant, J. Nelson, Quantifying Losses in Open-Circuit Voltage in Solution-Processable Solar Cells, PHYSICAL REVIEW APPLIED 4 (2015) 014020.

[43] R. Kotipalli, B. Vermang, J. Joel, R. Rajkumar, M. Edoff, D. Flandre, Investigating the electronic properties of Al2O3/Cu(In, Ga)Se_2 interface, AIP ADVANCES 5 (2015) 107101.

[44] R. Kotipalli, R. Delamare, O. Poncelet, X. Tang, L.A. Francis, and D. Flandre, Passivation effects of atomic-layer-deposited aluminum oxide, EPJ Photovoltaics 4 (2013) 45107.

[45] G. Sozzi, S. D. Napoli, M. Carrisi and R. Menozzi, "Assessing the impact of rear point-contact/passivation on CIGS cells with different absorber thickness and grading, 2018 IEEE 7th World Conference on Photovoltaic Energy Conversion (WCPEC) (A Joint Conference of 45th IEEE PVSC, 28th PVSEC & 34th EU PVSEC), Waikoloa Village, HI, (2018) 3044-3047.